6B.9 **A NEW WAY TO INVESTIGATE DYNAMICS IN A STORM USING DOPPLER SPECTRA FROM WEATHER RADAR**

Tian-You Yu[1,3]*, R. Reinoso-Rondinel[1,3], and R. D. Palmer[2,3]
[1] School of Electrical & Computer Engineering, Univ. of Oklahoma, Norman, Oklahoma.
[2] School of Meteorology, Univ. of Oklahoma, Norman, Oklahoma.
[3] Atmospheric Radar Research Center, Univ. of Oklahoma, Norman, Oklahoma

1. Introduction

Weather radar has been used widely not only for operationally monitoring and issuing warning of severe and hazardous weathers but also for providing important measurements to advance our understanding of the atmosphere (e.g., Serafin and Wilson 2000; National Research Council 2002). Reflectivity, mean radial velocity, and spectrum width are the three fundamental radar measurements, which are defined from the zeroth, first, and second moments of a Doppler spectrum (Doviak and Zrnić 1993). For weather radar the three spectral moments are often obtained using the autocovariance method because of its robustness and efficiency (e.g, Sirmans and Bumgarner 1975). In the autocovariance method, although the computation of Doppler spectrum is not needed, a model of Gaussian spectrum is used to derive the estimators of mean velocity and spectrum width. In other words, a bias in velocity and spectrum width can be resulted if the Doppler spectrum is deviated from symmetry and Gaussian, respectively.

In this work spectra from a tornadic supercell thunderstorm will be examined. Spectra deviated from Gaussian with dual-peak or strong tail can be observed. A spectrum model based on a mixture of two Gaussian functions is introduced and the power, mean velocity, and spectrum width from each Gaussian component are obtained using a non-linear fitting. The bias of velocity and spectrum width for the autocovariance method is derived based on such a model. Furthermore, spectra from a tornadic supercell, collected by the research WSR-88D (KOUN), are shown. Discussions of underlying processes to produce observed non-Gaussian spectra are included.

*Corresponding Author: T.-Y. Yu (tyu@ou.edu), School of Electrical and Computer Engineering, University of Oklahoma, Norman, OK 73019, USA

2. Model of Doppler spectrum

A Doppler spectrum $S(v)$ is defined as power weighted velocity distribution within the radar resolution volume. The value of $S(v)dv$ represents the return power of scatterers with radial velocity between v and $v + dv$ which is weighted by range weighting function and two-way antenna pattern. A Gaussian-shaped Doppler spectrum is typically assumed for weather signals and can be fully characterized by its three spectral moments of signal power, mean velocity, and spectrum width. However, the three moments are not sufficient to describe the spectrum shape if a spectrum is deviated from Gaussian. For example, a bimodal spectral signature caused by vortex can be observed from a tornadic region (e.g., Zrnić and Doviak 1975; Zrnić et al. 1985) and spectra with multiple patterns from insects, birds, and clea-air observed by weather radar were reported (Bachmann and Zrnić 2007). Moreover, it is of interest to quantify the bias error of the autocovariance method if a Doppler spectrum is deviated from Gaussian.

It is assumed that the model of Doppler spectrum consists of two Gaussian-shaped components as shown in the following form.

$$\begin{aligned} S(v) &= \frac{S_1}{\sqrt{2\pi}\sigma_1}\exp\left[-\frac{(v-v_1)^2}{2\sigma_1^2}\right] \\ &+ \frac{S_2}{\sqrt{2\pi}\sigma_2}\exp\left[-\frac{(v-v_2)^2}{2\sigma_2^2}\right] \end{aligned} \quad (1)$$

where S_i, v_i, and σ_i, $i = 1, 2$ are the signal power, mean velocity and spectrum width of each Gaussian component. Although a general case of n Gaussian components can be reconstructed, the

number of variables needed to defined such a spectrum increases as $3n$. In addition, spectra from the supercell storms we have observed did not show three prominent peaks. The total signal power of the dual-Gaussian spectrum is obtained by the zeroth moment $P = S_1 + S_2$. Moreover, the normalized Doppler spectrum $S_n(v) = S(v)/P$ is a mixture of two Gaussian probability density functions (pdfs) and its moments has been derived in the literature (e.g., Everitt and Hand 1981). The first moment and second central moments are obtained by the following equations.

$$v_r \equiv \int v S_n(v) dv = P_1 v_1 + P_2 v_2 \quad (2)$$

$$\sigma_v^2 \equiv \int (v - v_r)^2 S_n(v) dv = P_1 \sigma_1^2 + P_2 \sigma_2^2 + (v_2 - v_1)^2 P_1 P_2 \quad (3)$$

where $P_1 = S_1/P$ and $P_2 = S_2/P$. The mean velocity of the dual-Gaussian spectrum is defined by the first moment and is a weighted average of the mean velocities from each Gaussian moment. In addition, the spectrum width (σ_v) is defined by the square root of the second central moment, which depends on the weighted average of the spectrum widths from individual Gaussian and the separation of the their mean velocities. Hereafter, the spectral moments are referred to those of the dual-Gaussian model rather than a single Gaussian components except specified otherwise.

a. *Bias of spectral moments estimated by the autocovariance method*

Given the dual-Gaussian spectrum, its autocorrelation function is the superposition of the inverse Fourier transform of each individual Gaussian component as shown in the following form.

$$R(m) = S_1 \exp\left[-4(\frac{\pi\sigma_1 m}{v_a})^2\right] \exp\left[-j\frac{\pi v_1 m}{v_a}\right] + S_2 \exp\left[-4(\frac{\pi\sigma_2 m}{v_a})^2\right] \exp\left[-j\frac{\pi v_2 m}{v_a}\right] \quad (4)$$

where m is the temporal lag and $v_a = \lambda/(4T_s)$ is the maximum unambiguous velocity, T_s is the pulse repetition period and λ is the radar wavelength. In the autocovariance method, the mean velocity is estimated from the argument of the autocorrelation at lag one. As a result,

$$\hat{v}_r = \frac{v_a}{\pi} \arg R(1) = \frac{v_a}{\pi} \tan \frac{\sum_i A_i \sin\phi_i}{\sum_i A_i \cos\phi_i}, \quad (5)$$

where $R(1)$ is obtained from (4) with $m = 1$. As a result, $A_i = S_i \exp\left[-4(\frac{\pi\sigma_i}{v_a})^2\right]$ and $\phi_i = \frac{\pi v_i}{v_a}$, i=1 and 2 can be derived. Furthermore, the spectrum width can be estimated from the autocorrelation function at lags zero and one using the following form.

$$\hat{\sigma}_v = \frac{\sqrt{2} v_a}{\pi} \left| \ln\left(\frac{R(0)}{|R(1)|}\right)\right|^{1/2}. \quad (6)$$

where total signal power $R(0)$ equals to $S_1 + S_2$ from (4).

The signal power estimated from the autocorrelation at zero lag is an unbiased estimator. The theoretical bias of the velocity estimate for autocovariance method is defined by $b(\hat{v}_r) = E\{\hat{v}_r\} - v_r$, where $\hat{v}_r$ and v_r are given in (5) and (2), respectively. The ensemble mean is denoted by $E\{\ \}$. In addition, the bias of spectrum width is defined by $b(\hat{\sigma}_v) = E\{\hat{\sigma}_v\} - \sigma_v$ and $\hat{\sigma}_v$ and σ_v are given in (6) and (3). The bias of velocity and spectrum width estimators depends on the spectral moments of both Gaussian components, but their relationship is not clearly shown in above equations. It is important to point out that if spectral moments of both Gaussian components are of interest, the autocovariance estimators only provide a weighted average as shown in (2) and (3) even though they are unbiased.

b. *Dual-Gaussian moments estimation*

In this work, the six spectral moments from both Gaussian components are estimated by minimizing the mean squared errors (MSE) between the model spectrum of (1) and observed spectrum, defined in the following equation.

$$\varepsilon^2 \equiv \frac{1}{M} \sum_v \left| 10\log 10\left[\hat{S}(v)\right] - 10\log 10\left[S(v)\right]\right|^2 \quad (7)$$

where $\hat{S}(v)$ is the estimated Doppler spectrum and M is the number of samples for the estimation. Note that the MSE is defined in dB scale to suppress inherent statistical fluctuations in the spectral estimation. The minimization is solved using a Gaussian-Newton method with Levenberg-Marquardt modification (Seber and Wild 2003). Consequently, a dual-Gaussian spectrum can be reconstructed using estimated spectral moments.

3. Experimental Results

As discussed earlier, the dual-Gaussian fitting algorithm is most advantageous when the Doppler

spectrum is deviated from Gaussian shape and can be characterized by a mixture of two Gaussian functions. In addition, spectral moments of each component can be obtained, while the conventional autocovariance method is limited and can be biased. In this section, the dual-Gaussian fitting algorithm is demonstrated using spectra observed by the research WSR-88D (KOUN) operated by the National Severe Storms Laboratory (NSSL) in Norman, Oklahoma. KOUN has typical spatial resolution of 1 degree in angle and 250 m in range and it has the unique capability of continuously collecting time series of in-phase and quadrature signals for several hours. Time series data from a supercell thunderstorm in central Oklahoma on 10 May 2003 were collected. The fields of reflectivity, mean radial velocity, and spectrum width from elevation angles (ϕ) of 0.5 $^\circ$ at approximately 0405 UTC are presented from the left to the right columns in Fig. 1, respectively. In addition, the top and bottom rows are those fields from elevation angles (ϕ) of 1.5 $^\circ$ and 0.5 $^\circ$, respectively. The KOUN is located at the origin and all the results associated with reflectivity less than 20 dBZ are not shown for clarity. Evident signatures of hook-shape reflectivity and strong in-bound and out-bound velocities can be observed at 25 km east and 40 km north of KOUN, indicating the presence of a tornado. In addition, large spectrum widths can be observed in this region, which has been incorporated into a artificial intelligent algorithm to improve tornado detection (Wang et al. 2008). Generally speaking, these fields from the consecutive elevation scans exhibit fair continuity (not shown), except for a region of enhanced spectrum widths (> 6 m s^{-1}) only at the lowest elevation angle of 0.5 $^\circ$, which appears as a fan shape on the northeast of hook echoes. It has been reported that the median spectrum width from isolated tornadic storms has values small than 2 m s^{-1}(Fang et al. 2004). Therefore, it is of interest to investigate why spectrum widths in this region are much enhanced.

Spectra from azimuthal angle (θ) of 35 $^\circ$ and ranges between 55 to 75 km, that is depicted by the line $\overline{AB}$ in Fig. 1, are shown in the last column of Fig. 2 for both elevation scans. Spectra were initially obtained using the periodogram method with von Han window to increase the dynamic range (Doviak and Zrnić 1993). To reduce statistical fluctuations, spectra were subsequently averaged in range by a running window with a size of 8 gates (i.e., 2 km). Averaged spectra from every other six gates are displayed in dB in the third column of Fig. 2 with solid lines indicating those from elevation angle of 0.5 $^\circ$ and dash-dotted lines denoting those from $\phi = 1.5$ $^\circ$. The maximum unambiguous velocity (v_a) is approximately 32 m s^{-1}. Note that the autocorrelation functions were also smoothed using the same scheme of averaging. The fields of mean velocity and spectrum width shown in Fig. 1 were those obtained by the autocovariance method with the range-averaged autocorrelation functions. At each range gate, a Gaussian-shape spectrum can be reconstructed using the three spectral moments estimated by the autocovariance and is denoted by $S_a(v)$. Moreover, the dual-Gaussian fitting algorithm was applied to the averaged spectrum and consequently to obtain its reconstructed spectrum $S_d(v)$. Those results are shown in the first and second columns for the two elevation scans, respectively. Averaged-spectra shown in the third column are also included and denoted by dotted line. It is apparent that observed spectra can be better characterize by the dual-Gaussian model for both scans. Note that spectra at $\phi = 0.5$ $^\circ$ posses signatures of broad spectrum with relatively flat-top or dual-peak pattern and they become narrower with increasing range. These spectra can be reconstructed by two Gaussians with distinct mean velocities but comparable power. It is also evident that the autocovariance method tends to overestimate the spectrum width and provide mean velocities approximately between the locations of the two peaks, as shown in the first column of Fig. 2. For the case of $\phi = 1.5$ $^\circ$, spectra exhibit signatures of a single dominant peak and sometimes with tails such as those from ranges between 60 km and 68 km. In the dual-Gaussian model, the dominant peak is characterized by a strong and narrow Gaussian component and the tail can be described by the second component with smaller power and larger spectrum width. As a result, the autocovariance method can estimate the mean velocity of the dominant component but has the tendency to overestimate its spectrum width as the tail becomes stronger, as demonstrated by those spectra between of 60 km and 70 km. As spectra become more Gaussian-like between 72 and 76 km, the difference of reconstructed spectra from the autocovariance and dual-Gaussian fitting methods becomes smaller. Another interesting result is that spectra from $\phi = 1.5$ degr seem to relate to the right portion of the spectra at $\phi = 0.5$ $^\circ$, which can be exemplified by the spectra between 65 km and 70 km as shown in the rightmost column of Fig. 2. Hypothesis of the underlying processes to produce spectra from the two consecutive elevation scans will be discussed later.

To further investigate spectral moments esti-

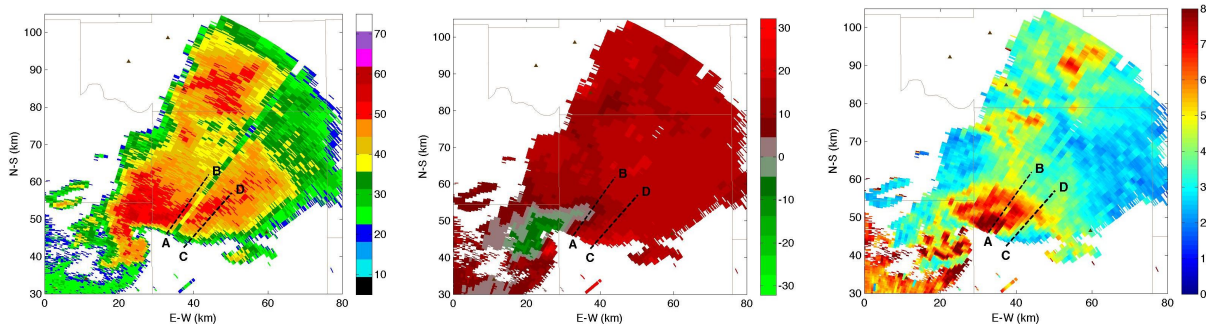

Figure 1: The fields of reflectivity, mean velocity and spectrum width from KOUN radar at the lowest elevation angle of 0.5 ° and 0405 UTC 10 May 2003 are shown from left to right panels, respectively.

mated from the autocovariance method and dual-Gaussian fitting method, we define the two Gaussian components: $S_1(v)$ is the one with larger mean velocity and $S_2(v)$ is the other one. In other words, $S_1(v)$ in Fig. 2 represents the right component of a spectrum. The estimated signal power, mean velocity and spectrum width of both components as a function of range are shown in Fig. 3 for both elevation angles. Spectral moments of $S_1(v)$ and $S_2(v)$ are denoted by green and red lines, respectively, and those from autocovariance method are indicated by blue solid lines. The estimated signal power, mean radial velocity, and spectrum width from $S_i(v)$ are denoted by $\hat{S}_i$, $\hat{v}_i$, and $\hat{\sigma}_i$, $i = 1$ and 2, respectively, and the three moments estimated by the autocovariance method are denoted by $\hat{S}$, $\hat{v}_r$, and $\hat{\sigma}_v$. It is shown that $\hat{S}_1$ and $\hat{S}_2$ are comparable with a maximum difference of 8.5 dB at approximately 63.4 km. In the top second column, the mean velocities estimated by the autocovariance method $\hat{v}_r$ have values between those from the two Gaussian components, $\hat{v}_1$ and $\hat{v}_2$. As discussed in section 2, the mean velocity of a dual-Gaussian spectrum is a weight average of the mean velocities from each component. The autocovariance method would provide such an estimate if the spectrum is symmetry. The weighted mean velocity, defined by $\overline{v}_r = (\hat{S}_1\hat{v}_1 + \hat{S}_2\hat{v}_2)/(\hat{S}_1 + \hat{S}_2)$ is also included and is depicted by a blue dashed line. Good agreement between $\overline{v}_r$ and $\hat{v}_r$ suggests that the bias in velocity estimate from the autocovariance method is relatively small. In addition, spectrum widths from the two Gaussian components have comparable magnitude of 2-3 m s^{-1}between 60 and 73 km, while the spectrum widths from the autocovariance method have values that are approximately doubled.

For $\phi = 1.5$ °, $S_1(v)$ usually represents the Gaussian component with dominant peak and $S_2(v)$ describes the tail. It appears clearly that $S_2(v)$ has signal power approximately 20 to 30 dB lower than the one of $S_1(v)$ and has relatively large spectrum width between 57 km and 71 km. The abrupt change of signal power and spectrum width at approximately 73.8 km and 75 km occurs when the two components has crossed over. Although the two Gaussian components can be assigned based on their estimated signal power to avoid such a problem, the mean velocities from the two components on the other hand will show these abrupt changes. As a result, the relationship of mean velocities from autocovariance method and dual-Gaussian fitting method is not as clear as the one in the figure. For the autocovariance-dreived mean velocities from 1.5 °, they are determined by the stronger component $S_1(v)$. The weighted mean velocity $\overline{v}_r$ also agrees well with $\hat{v}_r$, which is also suggested by symmetric spectra in Fig 2.

Furthermore, let's investigate what is responsible for the dual-Gaussian spectra at $\phi = 0.5$ ° and how they are related to spectra from a higher elevation scan. A dual-peak pattern can be obtained if two independent processes are present simultaneously within the radar resolution volume. For example, for a VHF or UHF profiler radar, dual-Gaussian spectra can be resulted from both precipitation and clear-air echoes that have different mean velocities (e.g., Boyer et al. 2003, 2004). For weather radar, spectra with a dual-peak signature were simulated and observed from tornadic vortices when the radar volume is sufficiently large to encompass both the inbound and outbound radial components and no significant velocity aliasing occurs (e.g., Zrnić and Doviak 1975; Bluestein et al. 1997; Yu et al. 2007). However, the region of interest is fairly large and is not in the vicinity of the tornado. Nevertheless it gives the idea that strong shears have the potential to produce such a spectral signature. Since the dual-peak or sometimes the flat-top spectra are ob-

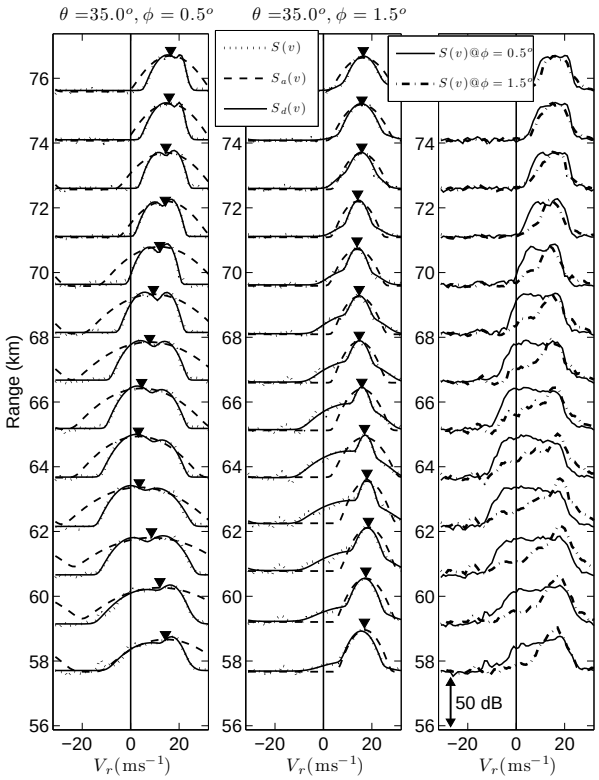

Figure 2: The first and second column are the averaged spectra ($S(v)$), denoted by dashed lines, at the azimuth of 35 ° for the two consecutive elevation angles, respectively. The spectra reconstructed using moments from the autocovariance method and dual-Gaussian fitting algorithm are defined by $S_a(v)$ and $S_d(v)$, as depicted by dotted and solid lines, respectively. In each panel, spectra are shown every 1.5 km after a range average of 2 km. It is evident that dual-peak or flat-top spectra can be observed from elevation $\phi = 0.5$ °, which generally are better characterized by the dual-Gaussian model. Observed spectra from ϕ =0.5 ° and 1.5 ° shown in the first two columns are overlaid in the third column with solid lines denoting spectra at $\phi = 0.5$ ° and dash-dotted lines representing those at 1.5 °. All spectra are shown in a dB scale. The mean velocities estimated by the autocovariance method are denoted by the location of downward triangles.

served in a number of consecutive radials, it is not likely such a shear pattern can repeatedly occur in the azimuthal direction. Therefore, the shear should be likely in the vertical direction. Indeed, it has been shown that vertical shear plays an important role in convective storms (e.g., Weisman and Klemp 1982; Weisman and Rotundo 2000). It should be noted that different combinations of reflectivity and velocity distributions can produce a similar spectrum. Therefore, it is not our goal to retrieve the velocity and reflectivity distribution from spectra. Instead, we are in an attempt to quantitatively show what a reasonable distribution of radial velocity and reflectivity can produce those observed spectra. Since only the vertical direction is of interest, mathematically the spectrum can be simplified to a 1D case as shown in the following formula (Doviak and Zrnić 1993).

$$S(v) = \int_{v=\eta} C f_b^4(\phi) Z(z) |\nabla v(z)|^{-1} dz. \qquad (8)$$

where $f_b^4(\phi)$ is the two way beam pattern in the elevation direction, $Z(z)$ and $v(z)$ are the reflectivity and radial velocity in the vertical direction, and C is a parameter that is a function of radar wavelength, peak transmitted power, range, antenna gain, and range weighting function. From (8) $S(v)dv$ represents the return power from all scatterers with radial velocity between v and $v+dv$ and is obtained by numerical simulations in this work. We use the simulation scheme similar to the ones used in Bluestein et al. (1993) and Yu et al. (2007). Initially the reflec-

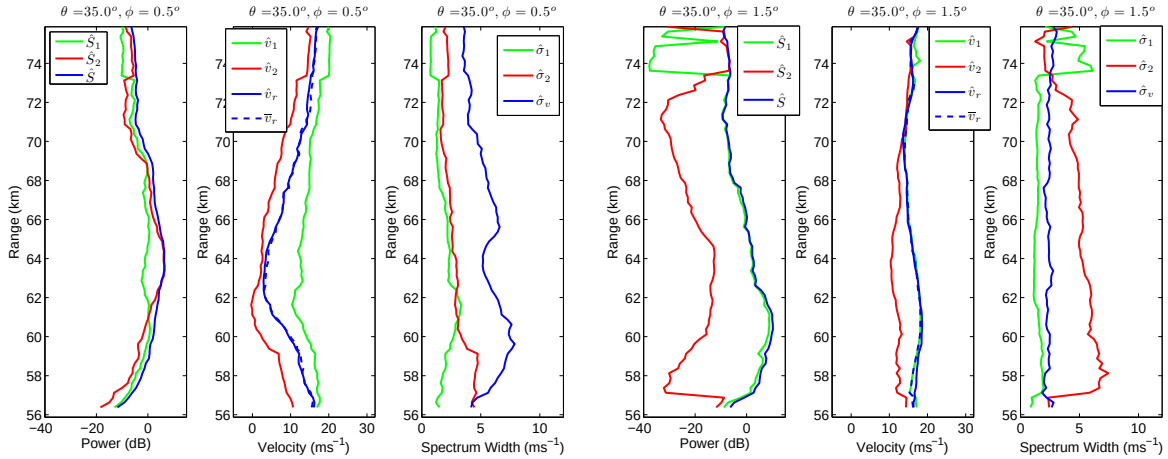

Figure 3: Range profiles of the spectral moments estimated by both autocovariance method and dual-Gaussian fitting technique. The first three plots from left to right are signal power, mean velocity, and spectrum width from azimuth of 35 ° and elevation of 0.5 ° . The second three plots are those from the same azimuth but the subsequent elevation angle of 1.5 ° . Spectral moments of $S_1(v)$ and $S_2(v)$ estimated from the dual-Gaussian fitting algorithm are depicted by red and green lines, respectively. Moments obtained by the autocovariance method are denoted by blue lines.

tivity and velocity are sampled at a finer scale. A Gaussian-shaped beam pattern from (11.117a) in Doviak and Zrnić (1993) is used with a half power beamwidth of 1 degree. The height of each ray path is calculated using $h = \sqrt{r^2 + R'^2 + 2rR' \sin\phi} - R'$, where the range $r = 65$ km, R' is 4/3 of the earth radius, and ϕ is the elevation angle of each ray path. The integration in (8) is subsequently performed by a summation of return power at heights with velocities between v and $v + dv$ over the radar volume, which is defined by the angle between -2 ° and 2 ° from the center of radar beam.

In order to obtain some ideal of a shear pattern, we first examine the relationship of spectra between $\phi = 0.5$ ° and 1.5 ° from the third column of Fig. 2. It appears that $S_1(v)$ maintains fairly good consistency from the two consecutive elevation scans, which suggests that the shear pattern responsible for $S_1(v)$ at $\phi = 0.5$ ° could occur in the upper portion of the beam and continuously extend to higher altitudes. Additionally, the velocities at the lower portion of the beam from $\phi = 0.5$ ° are smaller in order to produce $S_2(v)$ with smaller mean velocity. The profile of radial velocity is modeled using $v_r = v_s \tanh z/z_s$, which is the same formula as the one used in Weisman and Klemp (1982). We also set $v_s = 20$ m s^{-1}and $z_s = 800$ m. The profile is shown in the upper first panel of Fig. 4. Additional velocity fluctuations generated from a normal distribution with a standard deviation of 2 m s^{-1}was added. Two cases of reflectivity profiles presented in the second column were used in simulations and the resulted spectra are shown in the lower two panels. For each case, spectra at both $\phi = 0.5$ ° and 1.5 ° are generated and spectra with dual-peak signature are obtained from 0.5 ° for both cases. For case I both components of the dual-peak pattern have comparable power and for case II $S_1(v)$ (the one with larger mean velocity) has relatively large power, which are similar to some of the observed spectra. Moreover, spectra at 1.5 ° exhibit tail signature and their strong components are similar to the right component of the spectra ($S_1(v)$) at 0.5 ° . Note that a Doppler spectrum represents a weighted velocity distribution within the radar volume. In other words, the velocity profile determines the radial components in a spectrum. Additionally, the shape of spectrum is determined by the effective weighting function, which is defined by the product of reflectivity and beam pattern ($W \equiv fb^4(z)Z(z)$) and is shown in the top third column for both cases. The ordinate on the right represents corresponding elevation angles, where the center of the two beam locations are denoted by two arrows. Their height are approximately 0.86 and 2.05 km, respectively. It can be observed that the effective weighting function shows a dual-peak pattern for $\phi = 0.5$ ° for both cases. In addition, it is apparent that more retuned power comes from the lower portion of beam (where smaller velocities occur) in case I than those in case II. Moreover, it is hypothesized that the spectrum's

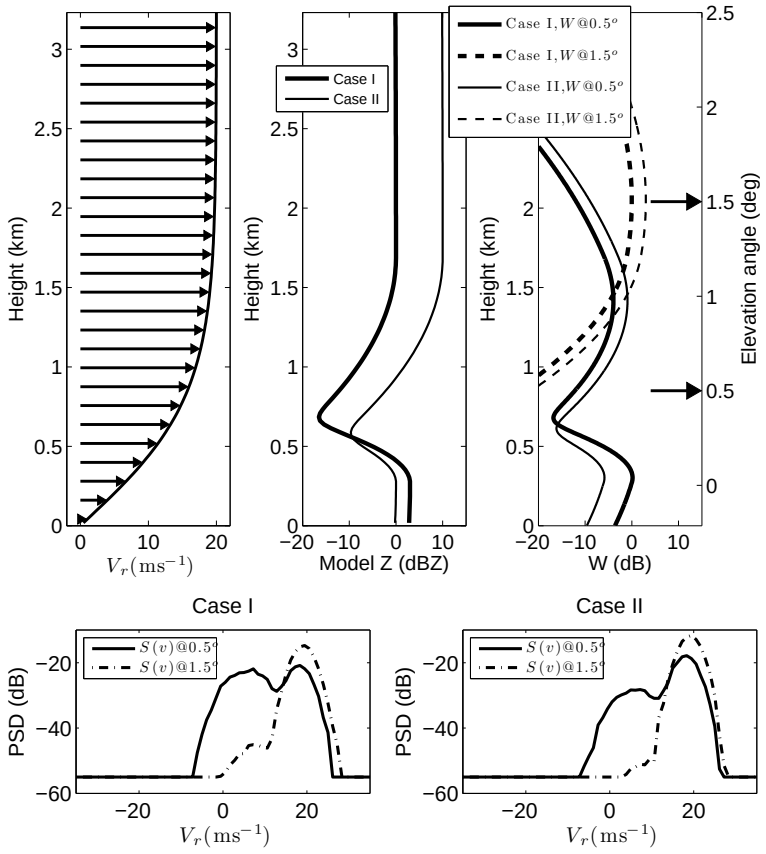

Figure 4: On the top panels from left to right are the profiles of radial velocity, reflectivity, and effective weighting (i.e., the product of reflectivity and radar beam pattern), respectively. The lower two panels are the spectra from the two cases. In each panel, spectra from the two consecutive scans are shown, which are similar to observed spectra.

tail at 1.5 ° are partially contributed by the scatterers from a lower altitude through the beam pattern. The power is only decreased by 3 dB at $\phi = 0.5$ ° from the radar beam centered at 1.5 °. Note that the tail is not symmetrical as those from observations. To produce such a result, more complicated radial velocity profile is needed and probably cannot be modeled by a simple mathematical equation. Nevertheless, our simple approach can produce spectra that are similar to observed spectra to some extent. Furthermore, those dual-peak spectra cannot be better characterized by a dual-Gaussian model as shown previously.

4. Conclusions

In this work, a dual-Gaussian model is introduced and each component is defined by three spectral moments. The mean power, Doppler velocity, and spectrum width of such a spectrum are derived in terms of the three spectral moments from each components. Theoretical bias of mean radial velocity and spectrum width estimated by the autocovariance method in relation to the six parameters are derived. Spectra from a supercell thunderstorm collected by the KOUN radar in Norman, Oklahoma are shown. Interesting spectra with dual-peak or flat-top are observed at the lower elevation angle of 0.5 °, which caused autocovariance method to overestimate the spectrum widths. At the consecutive higher elevation scan, spectra are correlated well with one of the component of the spectra from the lower elevation scan. In addition, tails are often observed for those spectrum which seemed to related to another component of the spectrum at the lower scan. Hypothesis of vertical shear pattern with enhanced reflectivity structure at lower altitudes is proposed. Spectra from hypothesized profile of reflectivity and radial velocity are simulated. Similar features to those from observations can be reproduced to some extent. More comprehensive analysis should be done using more sophisticated radar simulator and is planned. In addition, it is shown spectra can add an additional dimension and has the potential to reveal more detailed dynamics within the radar volume.

Acknowledgement This work was primarily supported by NOAA/NSSL under cooperative agreement of NA17RJ1227. Part of this work was supported in part by DOD, EPSCoR grant N00014-06-1-0590 and the National Science Foundation through ATM-0532107. The authors would also like to thank the technical support of NSSL in the collection of KOUN data.

References

Bachmann, S. and D. Zrnić, 2007: Spectral density of polarimetric variables separating biological scatterers in the VAD display. *J. Atmos. Oceanic Technol.*, **24**, 1185–1198.

Bluestein, H. B., J. G. Ladue, H. Stein, and D. Speheger, 1993: Doppler radar wind spectra of supercell tornadoes. *Mon. Wea. Rev.*, **121**, 2200–2221.

Bluestein, H. B., W. P. Unruh, and H. Stein, 1997: Doppler radar analysis of the Northfield, Texas, tornado of 25 May 1994. *Mon. Wea. Rev.*, **125**, 212–230.

Boyer, E., P. Larzabal, C. Adnet, and M. Petitdidier, 2003: Parametric spectral moments estimation for wind profiling radar. *IEEE Trans. Geosci. Remote Sens.*, **41**, 1859–1868.

Boyer, E., M. Petitdidier, and P. Larzabal, 2004: Stochastic maximum likelihood (SML) parametric estimation of overlapped Doppler echoes. *Ann. Geophy.*, **22**, 3983–3993.

Doviak, R. J. and D. S. Zrnić, 1993: *Doppler Radar and Weather Observations*. Academic, San Diego, Calif., 562 pp.

Everitt, B. S. and D. J. Hand, 1981: *Finite Mixture Distributions*. Chapman and Hall, Londom New York, 143 pp.

Fang, M., R. J. Doviak, and V. Melniko, 2004: Spectrum width measured by WSR-88D: Error sources and statistics of various weather phenomena. *J. Atmos. Oceanic Technol.*, **21**, 888–904.

National Research Council, 2002: *Weather Radar Technology beyond NEXRAD*. National Academies Press, Washington, D.C.

Seber, G. A. F. and C. J. Wild, 2003: *Nonlinear Regression*. Wiley, Hoboken, New Jersey, 768 pp.

Serafin, R. J. and J. W. Wilson, 2000: Operational weather radar in the United States: progress and opportunity. *Bull. Amer. Meteor. Soc.*, **81**, 501–518.

Sirmans, D. and B. Bumgarner, 1975: Numerical comparison of five mean frequency estimators. *J. Appl. Meteor.*, **14**, 991–1003.

Wang, Y., T.-Y. Yu, M. Yeary, A. Shapiro, S. Nematifer, M. Foster, D. L. A. Jr., and M. Jain, 2008: Tornado detection using a neuro-fuzzy yystem to integrate shear and spectral signatures. *J. Atmos. Oceanic Technol.*, **accpeted**.

Weisman, M. L. and J. B. Klemp, 1982: The dependence of numerically simulated convective storms on vertical wind shear and buoyancy. *Mon. Wea. Rev.*, **110**, 504–520.

Weisman, M. L. and R. Rotundo, 2000: The use of vertical wind shear versus helicity in interpreting supercell dynamics. *J. Atmos. Sci.*, **57**, 1452–1472.

Yu, T.-Y., Y. Wang, A. Shapiro, M. Yeary, D. Zrnić, and R. Doviak, 2007: Characterization of tornado spectral signatures using higher order spectra. *J. Atmos. Oceanic Technol.*, **in press**.

Zrnić, D. S., D. W. Burgess, and L. D. Hennington, 1985: Doppler spectra and estimated windspeed of a violent tornado. *J. Climate Appl. Meteor.*, **24**, 1068–1081.

Zrnić, D. S. and R. J. Doviak, 1975: Velocity spectra of vortices scanned with a pulsed-Doppler radar. *J. Appl. Meteor.*, **14**, 1531–1539.